METASURFACES

Plasmonic topological metasurface by encircling an exceptional point

Qinghua Song[1], Mutasem Odeh[2], Jesús Zúñiga-Pérez[1], Boubacar Kanté[2,3], Patrice Genevet[1]*

Resonant scattering, guided mode propagation phase, and/or orientation-dependent phase retardations are the three main mechanisms used to date to conceive optical metasurfaces. Here, we introduce an additional degree of freedom to address optical phase engineering by exploiting the topological features of non-Hermitian matrices operating near their singular points. Choosing metasurface building blocks to encircle a singularity following an arbitrarily closed trajectory in parameter space, we engineered a topologically protected full 2π-phase on a specific reflected polarization channel. The ease of implementation together with its compatibility with other phase-addressing mechanisms bring topological properties into the realm of industrial applications at optical frequencies and prove that metasurface technology represents a convenient test bench to study and validate topological photonic concepts.

Metasurfaces (*1*–*6*) are artificial materials constructed with subwavelength arrays of spatially distributed nanostructures that enable versatile wavefront engineering. From a fundamental perspective, a metasurface is an open system, continuously exchanging and/or absorbing energy between the impinging field and the resonant nanostructures. Unlike closed systems, open systems experience a phase transition at the exceptional point (EP), leading to complex scattering phenomena related to optical singularities (*7*). The latter can be equivalently described in an optical system by using the scattering matrix and Hamiltonian representations (*8*–*10*). Singularities also manifest in the reflection-zero regime, perfect absorption and bound state in the continuum, giving rise to, for example, unidirectional transmission or reflection (*11*, *12*), single-mode laser operation (*13*), and extreme sensitiveness to perturbation (*14*, *15*). Tailoring light reflection, or transmission, with metasurfaces consists in addressing the values of complex coefficients by varying the nanostructure geometries. Choosing any arbitrary loop in parameter space to achieve phase distribution does not necessarily lead to full 2π-phase accumulation. Here, we show how to leverage the 2π-phase excursion that occurs on the coefficient value by encircling zeros or singularities in the complex plane. Encircling a singular point to accumulate an optical phase difference is of crucial interest for wavefront engineering, enrichening the metasurface design toolbox with an additional phase-addressing mechanism.

[1]Université Côte d'Azur, CNRS, Centre de Recherche sur l'Hétéro-Epitaxie et ses Applications, Rue Bernard Gregory, Sophia Antipolis, 06560 Valbonne, France. [2]Department of Electrical Engineering and Computer Sciences, University of California, Berkeley, CA 94720, USA. [3]Materials Sciences Division, Lawrence Berkeley National Laboratory, Berkeley, CA 94720, USA.
*Corresponding author. Email: patrice.genevet@crhea.cnrs.fr

Previous works on metasurfaces have shown that non-Hermitian metasurfaces can operate close to an EP and have approached singularity owing to a series of individually distinct metasurfaces for which a given parameter is changed (*16*–*19*). The exploitation of the robust topological phase around the EP, referred to as the exceptional topological (ET) phase, to realize functional devices has remained elusive. The proposed ET phase is fundamentally different from the conventional Pancharatnam-Berry (PB) phase (*20*–*23*), and as a consequence, ET can be combined with other phase-addressing mechanisms, including PB, to achieve full and independent control of the polarization channels. We have demonstrated a meta-hologram by using the ET phase encircling the EP to project an image of "C" for left circular polarized (LCP) light, leaving the cross right circular polarized (RCP) channel unaffected. By combining the ET and PB phases, we decoupled the two circular polarizations (CPs) and achieved two different holographic projections with an image of "A" for LCP light and "B" for RCP light.

The plasmonic topological metasurface consists of three layers, where a dielectric layer is sandwiched between a metal ground and a metallic structured layer (Fig. 1A). The metal ground blocks all the transmission so that the metasurface works in the reflective regime. The structured layer is formed by a two-dimensional (2D) planar chiral structure array, which is composed of an "L"-shaped nanostructure, near-field coupled to a straight nanorod. To observe the EP complex-square-root topology of the eigenvalues surface, two parameters need to be varied, defining the parameter space $\boldsymbol{R} = (L_1, L_3)$, with L_1 and L_3 being the geometrical parameters shown in Fig. 1A. L_1 and L_3 were chosen because they play key roles in the y- and x-polarized resonances (fig. S9 and supplementary text S4), giving access to a full 2π reflection phase for r_{+-} [where the subscript +– represents reflected CP conversion from RCP ($|-\rangle$) to LCP ($|+\rangle$)]. The EP was obtained by adjusting the nanostructure structural properties, so that both eigenstates degenerate as CP beams. If the degenerate eigenstate is RCP—that is, $\hat{r}|-\rangle = \lambda_{1,2}|-\rangle$, where $\hat{r}$ is the reflection matrix and $\lambda_1 = \lambda_2$ are two degenerate eigenvalues—then RCP input light is preserved, and the CP conversion channel from RCP to LCP vanishes—that is, $r_{+-} = 0$. A zero point or singularity point, equivalent to perfect absorption cases (*24*–*26*), is obtained for r_{+-} (Fig. 1B). The chiral response of the surface current distribution at the EP (fig. S7) is a key ingredient to achieve CP-dependent reflectivity. The induced chirality is an inherent property of the EP from a symmetric non-Hermitian Hamiltonian (*27*) and leads to an asymmetric conversion from one CP to the other and vice versa ($r_{+-} \neq r_{-+}$). The spectral response of only one of the two CP conversions undergoes a 2π-phase change around the EP wavelength. Because of the topological protection provided by encircling of the EP (supplementary text S1 and S2), the 2π-phase accumulation is maintained for the reflected phase map irrespective of the closed path, as long as it encircles one EP in parameter space. Given the metasurface versatility, we realized on a single component an assembly of antennas with different parameters chosen so as to move around the EP in the parameter space, thus realizing simultaneously a set of optical responses (Fig. 1, G and J). We also observed amplitude variation with singular value. The other reflective CP conversion coefficient (r_{-+}) does not present a singularity in this parameter space, resulting in almost constant phase and amplitude profiles (Fig. 1C).

The conventional PB phase works oppositely for the two reflective CP conversion beams (Fig. 1, D to F). Being fundamentally different, the ET phase is imposed on only one CP conversion and thus can be combined with the standard PB phase (supplementary text S5). As a result, the combination of ET and PB phases can be used to decouple the phase of the two CP conversion beams, leading to independent control of each polarization-converted wavefront (Fig. 1, G to L).

A spectral singularity point of r_{+-}, together with its degeneracy of the eigenvalues and eigenstates at λ = 600 nm, prove the existence of an EP (Fig. 2, red star). This behavior was further confirmed by the intersecting double Riemann surface corresponding to the reflection matrix eigenvalues (Fig. 3, A and B). Various phase and amplitude-conversion distribution choices are possible for the deflecting unit cell. We chose a simple unit cell phase coverage, considering 90° phase steps, so as to keep the distance between neighboring antennas constant, which slightly compromises

the amplitude of the third structure (Fig. 3E). Seven designs of PB phase interval of 60° are also presented in Fig. 3, C to H, for combination with the ET phase.

We experimentally demonstrated an ET-phase gradient metasurface, behaving as a beam deflector and a meta-hologram. The scanning electron micrograph (SEM) of the fabricated beam deflector is shown in Fig. 4A. An asymmetric reflection of the two CP conversion beams is measured in Fig. 4B, with a maximum efficiency of 12% and power ratio around 10:1, as quantified in Fig. 4C. The spectral position of the singular design (EP antenna) evolves as a function of the antenna structural parameters (fig. S13), indicating that small nanofabrication errors can slightly shift the position of the EP and modify the expected deflection

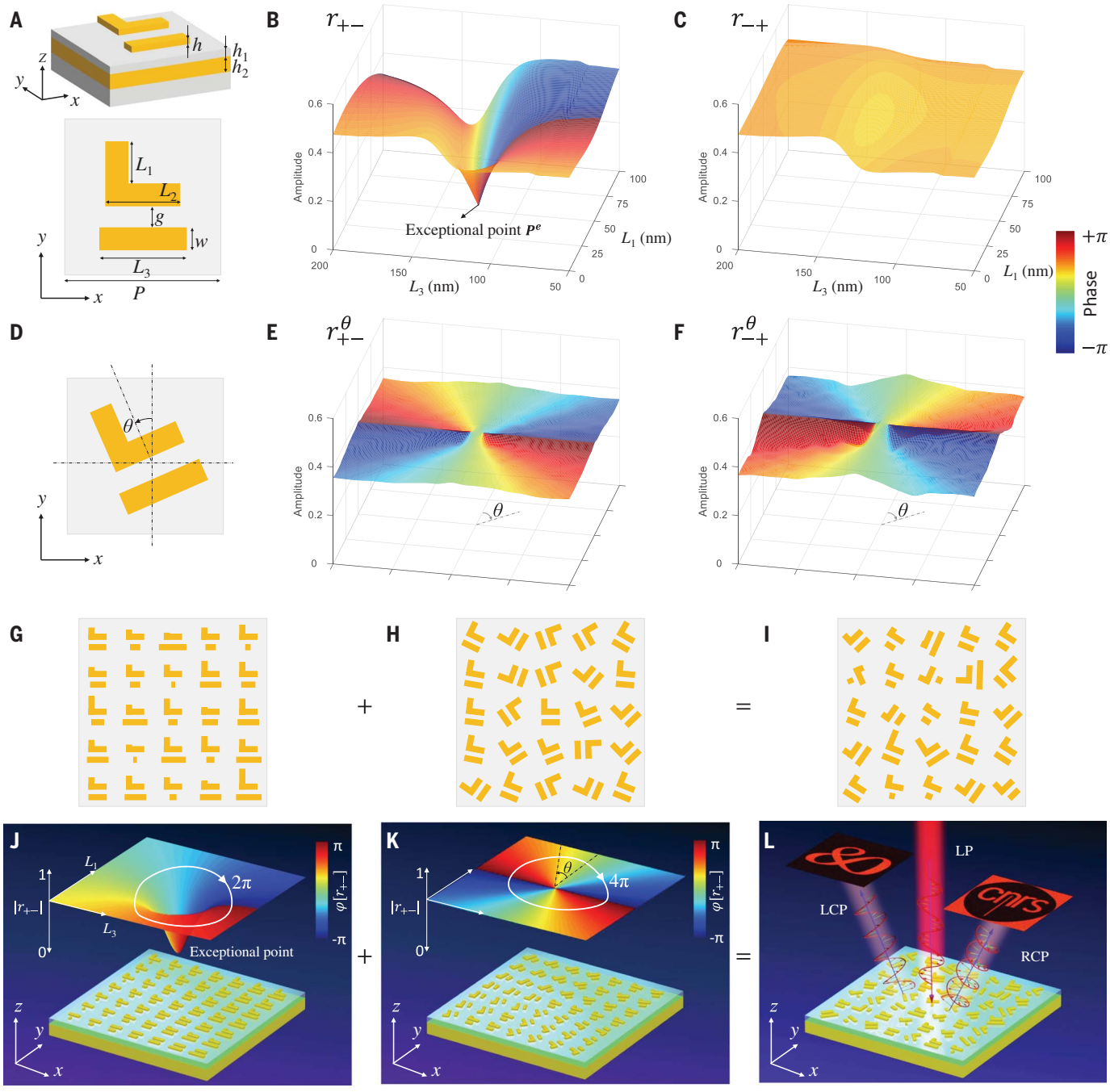

Fig. 1. Design principle of the topological metasurface. (**A**) (Top) Perspective and (bottom) top view of 2D chiral meta-atom design in reflection. The dimensions are L_2 = 140 nm, P = 300 nm, w = 50 nm, g = 70 nm, h = 30 nm, h_1 = 40 nm, and h_2 = 150 nm. (**B** and **C**) Simulated CP conversion coefficients (B) r_{+-} and (C) r_{-+} in the parameter space covered by $L_1 \in [0, 100\ \text{nm}]$ and $L_3 \in [50\ \text{nm}, 200\ \text{nm}]$. An EP is obtained at ($L_1$, L_3) = (52 nm, 119 nm). A vortex phase profile for r_{+-} and a topological protected 2π-phase accumulation is obtained by encircling the EP, as indicated in (B) by the full-color map coverage on the surface. (**D**) Top view of meta-atom with rotation angle of θ. (**E** and **F**) Simulated CP conversion coefficients (E) r^{θ}_{+-} and (F) r^{θ}_{-+} with $\theta \in [0, 2\pi]$. In (E) and (F), the original ET phase without rotation ($r^{0}_{\pm\mp}$) has been subtracted to display the PB phase only. The z axis in (B), (C), (E), and (F) indicates the amplitude, and the color scale indicates the phase. (**G** to **I**) The combination of (G) ET phase and (H) PB phase is designed to realize an (I) ET+PB phase metasurface. (**J** to **L**) Schematics of the design implemented for combining the (J) ET and (K) PB phase control in (L) a single ET+PB phase metasurface, able to independently control the two CP beams.

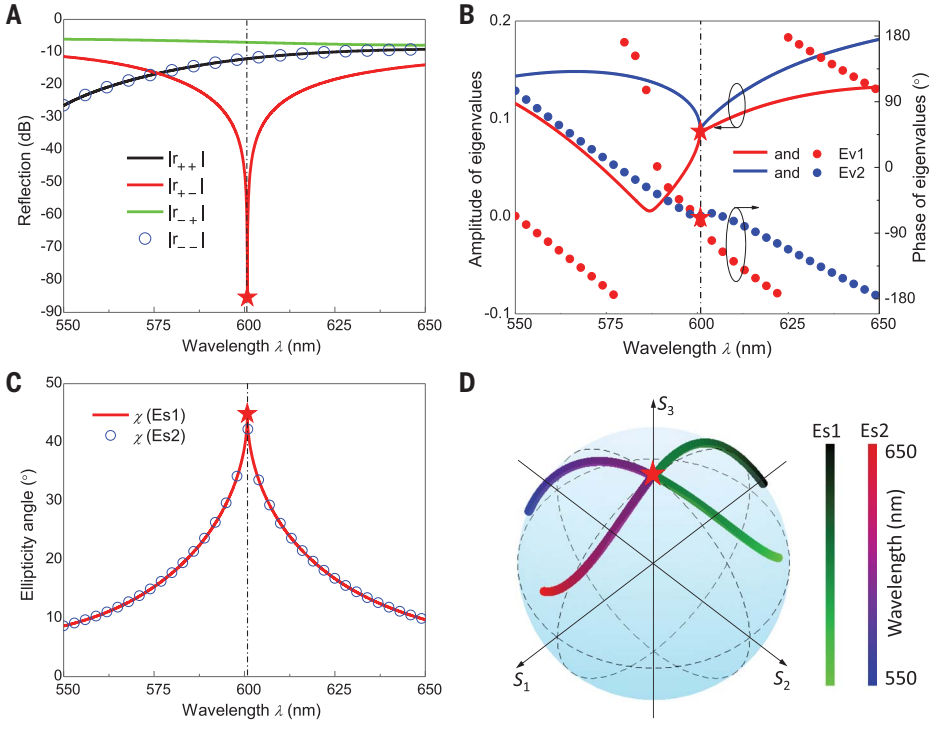

Fig. 2. Simulated reflection spectra and the corresponding eigenvalues and eigenstates. (**A**) Spectral dependence of the reflection matrix coefficients (in the circular basis). A singularity point, where $r_{+-} = 0$, is observed at λ = 600 nm. (**B**) Amplitude and phase of the reflection matrix eigenvalues. The two eigenvalues degenerate at λ = 600 nm. (**C**) Simulated ellipticity angle of the two eigenstates, which overlap and degenerate as RCP at λ = 600 nm. (**D**) Position of the eigenstates on the Poincaré sphere as a function of wavelength, which degenerate at λ = 600 nm. All of these features prove that an EP is obtained at λ = 600 nm.

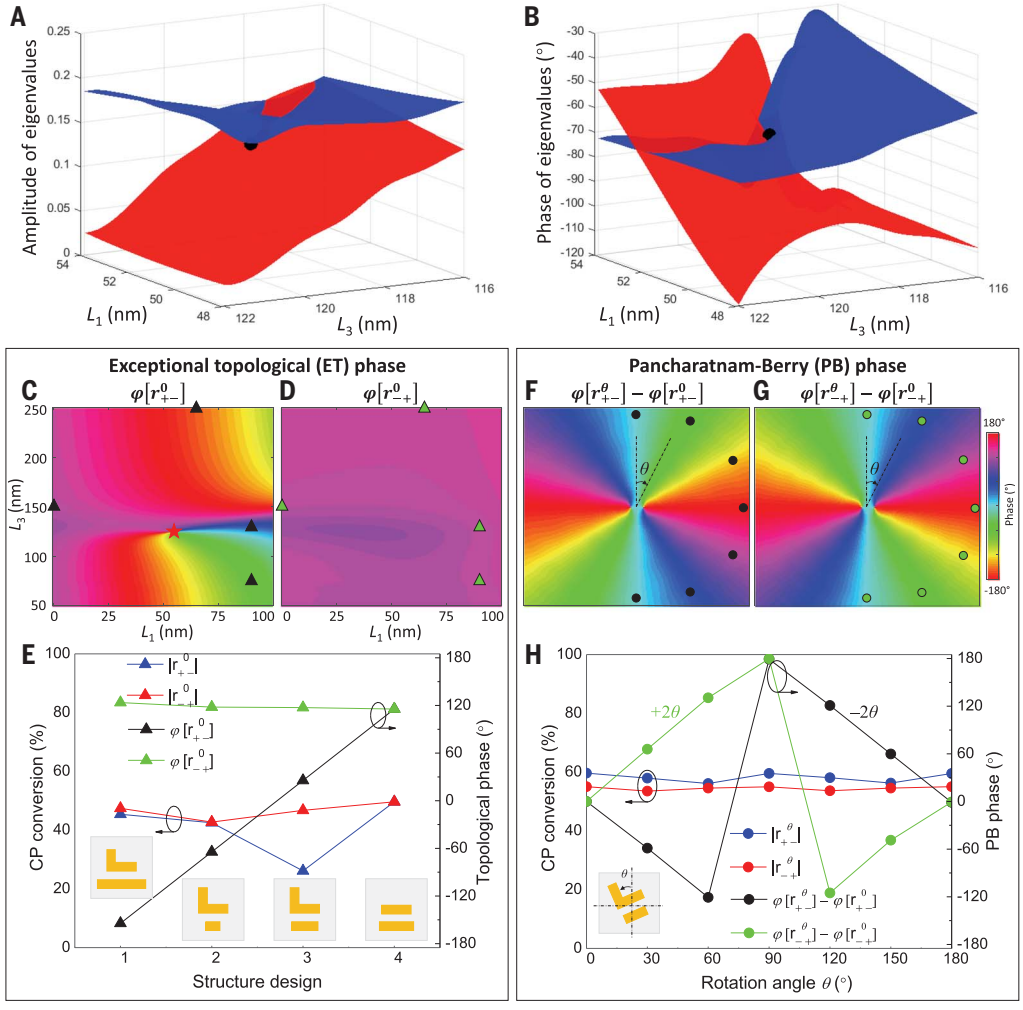

Fig. 3. Simulation results of the metasurface in the parameter space $R = (L_1, L_3)$. (**A**) Simulated amplitude and (**B**) phase of two eigenvalues at λ = 600 nm. A self-intersecting Riemann surface profile is observed. The EP is indicated with the black dot, where two eigenvalues degenerate at (L_1, L_3) = (52 nm, 119 nm). (**C**) Simulated ET phase of r^0_{+-} and (**D**) nearly constant phase of r^0_{-+}. (**E**) Four meta-atom designs are selected so that the ET phase interval is 90°, indicated with triangles in (C) and (D). (Insets) Four corresponding structure designs. (**F** and **G**) Simulated PB phase of (F) r^θ_{+-} and (G) r^θ_{-+} with (L_1, L_3) = (80 nm, 95 nm). where the presented phase has been subtracted by the original phase of $r^0_{\pm\mp}$ without rotation to display PB phase only. (**H**) Seven rotated structures are presented with rotation angle from 0° to 180° stepped by 30°, indicated with dots in (F) and (G) (figs. S11 and S14).

efficiencies and power ratio. To show the versatility of this wavefront phase encoding technique, we realized a meta-hologram (Fig. 4D). As expected, a holographic image of "C" is displayed for r_{+-} (Fig. 4E), but no image appears for r_{-+} (Fig. 4F).

The wealth of applications of the ET phase expands by combining it with other phase-control mechanisms. We combined ET with the widespread PB phase by simply rotating the metasurface elements (Fig. 4, G to L) to decouple the deflection angles of the two CP beams (Fig. 4, H and I). Similarly, we applied ET+PB phase encoding to project two different CP holographic images (Fig. 4, K and L).

We have demonstrated a planar chiral plasmonic metasurface that exhibits 2π topological phase accumulation in a reflection regime

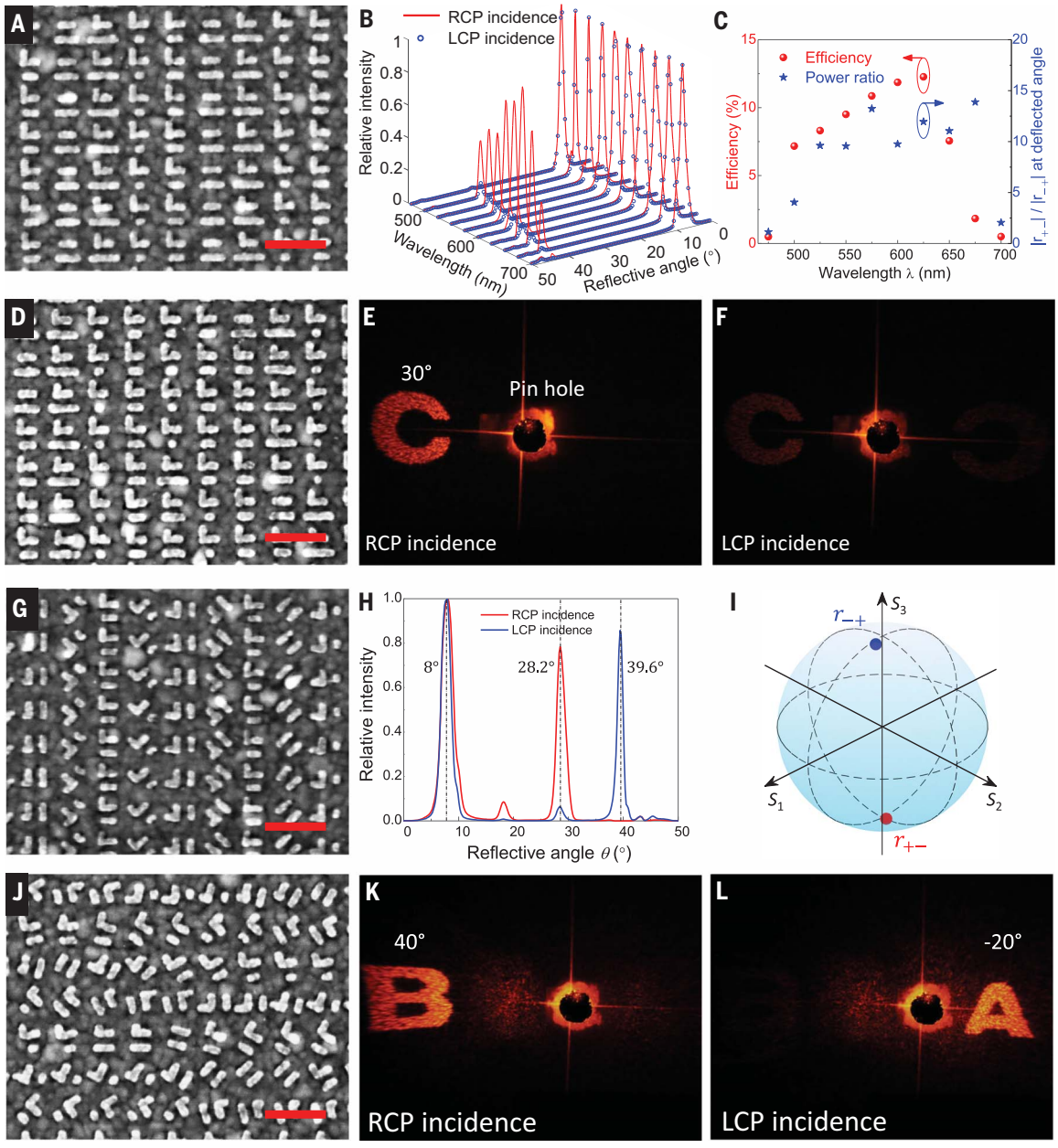

Fig. 4. Experimental results of the topological metasurface. (**A**) Fabricated nanostructures for the ET phase meta-deflector. (**B**) Measured far-field power patterns for RCP (red solid curves) and LCP (blue dotted curves) incidence on ET phase meta-deflector. The phase gradient between adjacent meta-atoms is designed as 90°. The first order of the CP-converted beam r_{+-} is deflected from 34° to ~44° when the wavelength λ varies from 500 to ~675 nm, whereas the other CP-converted beam of r_{-+} is undeflected (at the zero order of 8°). (**C**) Measured efficiency of the deflector (red dots) and measured power ratio of $|r_{+-}|/|r_{-+}|$ at the deflected angle (blue stars). (**D**) Fabricated nanostructures for an ET phase meta-hologram designed by encoding the holographic phase profile into the deflector. (**E**) A holographic image of "C" for r_{+-} is displayed at the angle of 30°, but (**F**) no image appears for r_{-+}. (**G**) Fabricated nanostructures for an ET+PB phase meta-deflector. (**H**) Measured far-field power patterns with RCP (red curve) and LCP (blue curve) incidence on ET+PB phase meta-deflector. The phase gradient between adjacent meta-atoms is designed as 60° and 90°, respectively for r_{+-} and r_{-+}. (**I**) Poincaré sphere representation of the measured polarization of r_{+-} (red dot) and r_{-+} (blue dot) at the first deflected order. (**J**) Fabricated nanostructures for an ET+PB phase meta-hologram. (**K** and **L**) Holographic images of (K) "B" for r_{+-} and (L) "A" for r_{-+} are displayed at the designed angle of 40° and −20°, respectively. All the curves in (B) and (H) are normalized with the zero order as unity. The operating wavelength in (E), (F), (H), (K), and (L) is λ = 600 nm. The incident angles of the deflectors and holograms are 8° and 0°, respectively. Scale bars, 500 nm.

by choosing nanoantenna designs distributed along any arbitrarily closed parameter loop encircling the EP. We have shown that 2π-phase accumulation is imposed on only one of the CP conversion beams defined by the chirality of the encircled EP. Exploiting a linear combination of ET and PB phases, we decoupled LCP and RCP channels. Addressing phase retardation by encircling singularities of the S-matrix opens vast research opportunities for linear and nonlinear topological electromagnetic field control at optical frequencies.

REFERENCES AND NOTES

1. N. Yu *et al*., *Science* **334**, 333–337 (2011).
2. P. Genevet *et al*., *Nat. Nanotechnol.* **10**, 804–809 (2015).
3. A. Alù, N. Engheta, *Nat. Photonics* **2**, 307–310 (2008).
4. Q. Song *et al*., *Nat. Commun.* **12**, 3631 (2021).
5. M. V. Gorkunov, A. A. Antonov, Y. S. Kivshar, *Phys. Rev. Lett.* **125**, 093903 (2020).
6. D. B. Haim, L. Michaeli, O. Avayu, T. Ellenbogen, *Opt. Express* **28**, 17923–17933 (2020).
7. W. D. Heiss, *J. Phys. A Math. Theor.* **45**, 444016 (2012).
8. W. R. Sweeney, C. W. Hsu, S. Rotter, A. D. Stone, *Phys. Rev. Lett.* **122**, 093901 (2019).
9. Ş. K. Özdemir, S. Rotter, F. Nori, L. Yang, *Nat. Mater.* **18**, 783–798 (2019).
10. M.-A. Miri, A. Alù, *Science* **363**, eaar7709 (2019).
11. A. Regensburger *et al*., *Nature* **488**, 167–171 (2012).
12. Z. Lin *et al*., *Phys. Rev. Lett.* **106**, 213901 (2011).
13. L. Feng, Z. J. Wong, R.-M. Ma, Y. Wang, X. Zhang, *Science* **346**, 972–975 (2014).
14. J.-H. Park *et al*., *Nat. Phys.* **16**, 462–468 (2020).
15. M. C. Rechtsman, *Nature* **548**, 161–162 (2017).
16. H. Alaeian, J. A. Dionne, *Phys. Rev. A* **89**, 033829 (2014).
17. X. Wang, X. Fang, D. Mao, Y. Jing, Y. Li, *Phys. Rev. Lett.* **123**, 214302 (2019).
18. M. Lawrence *et al*., *Phys. Rev. Lett.* **113**, 093901 (2014).
19. S. H. Park *et al*., *Nanophotonics* **9**, 1031–1039 (2020).
20. D. Lin, P. Fan, E. Hasman, M. L. Brongersma, *Science* **345**, 298–302 (2014).
21. G. Zheng *et al*., *Nat. Nanotechnol.* **10**, 308–312 (2015).
22. Q. Song *et al*., *Nat. Commun.* **11**, 2651 (2020).
23. Q. Song *et al*., *Sci. Adv.* **7**, eabe1112 (2021).
24. E. Plum, N. I. Zheludev, *Appl. Phys. Lett.* **106**, 221901 (2015).
25. X. Yang, M. Li, Y. Hou, J. Du, F. Gao, *Opt. Express* **27**, 6801–6814 (2019).
26. A. Krasnok *et al*., *Adv. Opt. Photonics* **11**, 892–951 (2019).
27. W. D. Heiss, H. L. Harney, *Eur. Phys. J. D* **17**, 149–151 (2001).

ACKNOWLEDGMENTS

Funding: P.G. acknowledges funding from the European Union's Horizon 2020 research and innovation program (grant agreement 639109). B.K. acknowledges funding from Office of Naval Research Young Investigator Award (N00014-17-1-2671) and the Laboratory Directed Research and Development Program of Lawrence Berkeley National Laboratory under the US Department of Energy (DE-AC02-05CH11231). **Author contributions:** Q.S., J.Z.-P., and P.G. conceived the initial ideas and carried out the experiment. Q.S. designed the structure and performed the numerical calculations. M.O. and B.K. fabricated the samples. P.G. supervised the research. All authors wrote the manuscript. **Competing interests:** The authors declare no competing financial interest. **Data and materials availability:** All data needed to evaluate the conclusions in the paper are available in the main text or the supplementary materials.

SUPPLEMENTARY MATERIALS

science.sciencemag.org/content/373/6559/1133/suppl/DC1
Materials and Methods
Supplementary Text S1 to S5
Figs. S1 to S14
References (*28*, *29*)

5 May 2021; accepted 3 August 2021
10.1126/science.abj3179

Science

Plasmonic topological metasurface by encircling an exceptional point

Qinghua SongMutasem OdehJesús Zúñiga-PérezBoubacar KantéPatrice Genevet

Science, 373 (6559), • DOI: 10.1126/science.abj3179

Upon reflection, modulate phase

Metasurfaces provide a platform to fabricate optical devices in a compact form much thinner than their corresponding bulk optical components. Recognizing that metasurfaces are also open systems interacting with their environment, Song *et al*. designed a metasurface that exploits those non-Hermitian properties such that they can encircle an exceptional point. Subsequent scattering from such an exceptional point was shown to be polarization dependent, thus providing an additional control knob in designing metasurfaces for wave front engineering. —ISO

Science (ISSN) is published by the American Association for the Advancement of Science. 1200 New York Avenue NW, Washington, DC 20005. The title *Science* is a registered trademark of AAAS.